

# Mid-infrared Fourier-transform spectroscopy with a high-brilliance tunable laser source: investigating sample areas down to 5 $\mu\text{m}$ diameter

T. Steinle,\* F. Neubrech, A. Steinmann, X. Yin, and H. Giessen

4th Physics Institute and Research Center SCoPE, University of Stuttgart, Pfaffenwaldring 57,  
70569 Stuttgart, Germany

\*[t.steinle@pi4.uni-stuttgart.de](mailto:t.steinle@pi4.uni-stuttgart.de)

**Abstract:** We demonstrate highly sensitive infrared spectroscopy of sample volumes close to the diffraction limit by coupling a femtosecond fiber-feedback optical parametric oscillator (OPO) to a conventional Fourier-transform infrared (FTIR) spectrometer. The high brilliance and long-term stable infrared radiation with  $1/e^2$ -bandwidths up to 125 nm is easily tunable between 1.4  $\mu\text{m}$  and 4.2  $\mu\text{m}$  at 43 MHz repetition rate and thus enables rapid and low-noise infrared spectroscopy. We demonstrate this by measuring typical molecular vibrations in the range of 3  $\mu\text{m}$ . Combined with surface-enhanced infrared spectroscopy, where the confined electromagnetic near-fields of resonantly excited metal nanoparticles are employed to enhance molecular vibrations, we realize the spectroscopic detection of a molecular monolayer of octadecanethiol. In comparison to conventional light sources and synchrotron radiation, our compact table-top OPO system features a significantly improved performance making it highly suitable for rapid analysis of minute amounts of molecular species in life science and medicine laboratories.

© 2015 Optical Society of America

**OCIS codes:** (190.4970) Parametric oscillators and amplifiers; (300.6340) Spectroscopy, infrared; (240.6490) Spectroscopy, surface; (250.5403) Plasmonics.

---

## References and links

1. M. Diem, M. Romeo, S. Boydston-White, M. Miljkovic, and C. Matthaus, "A decade of vibrational micro-spectroscopy of human cells and tissue (1994-2004)," *Analyst*, **129**, 880–885 (2004).
2. C. Petibois and G. M. Deleris, "Chemical mapping of tumor progression by FT-IR imaging: towards molecular histopathology," *Trends Biotechnol.* **24**, 455–462 (2006).
3. C. Petibois, G. Deleris, M. Piccinini, M. Cestelli-Guidi, and A. Marcelli, "A bright future for synchrotron imaging," *Nature Photon.* **3**, 179 (2009).
4. M. Martin, U. Schade, P. Lerch, and P. Dumas, "Recent applications and current trends in analytical chemistry using synchrotron-based Fourier-transform infrared microspectroscopy," *Trends Anal. Chem.* **29**, 453–160 (2010).
5. L. Novotny and N. van Hulst, "Antennas for light," *Nature Photon.* **5**, 83–90 (2011).
6. F. Neubrech, A. Pucci, T. W. Cornelius, S. Karim, A. Garcia-Etxarri, and J. Aizpurua, "Resonant plasmonic and vibrational coupling in a tailored nanoantenna for infrared detection," *Phys. Rev. Lett.* **103**, 157403 (2008).
7. R. Adato and H. Altug, "In-situ ultra-sensitive infrared absorption spectroscopy of biomolecule interactions in real time with plasmonic nanoantennas," *Nat. Commun.* **4**, 2154 (2013).
8. T. Wang, V. H. Nguyen, A. Buchenauer, U. Schnakenberg, and T. Taubner, "Surface enhanced infrared spectroscopy with gold strip gratings," *Opt. Express* **21**, 9005–9010 (2013).

9. P. Willmott, *An Introduction to Synchrotron Radiation: Techniques and Applications* (John Wiley & Sons, 2011).
10. P. Dumas, F. Polack, B. Lagarde, O. Chubar, J. Giorgetta, and S. Lefrancois, "Synchrotron infrared microscopy at the French synchrotron facility SOLEIL," *Infrared Phys. Technol.* **49**, 152–160 (2006).
11. Y. Yao, X. Wang, J.-Y. Fan, and C. F. Gmachl, "High performance 'continuum-to-continuum' quantum cascade lasers with a broad gain bandwidth of over  $400\text{ cm}^{-1}$ ," *Appl. Phys. Lett.* **97**, 081115 (2010).
12. Y. Yao, A. J. Hoffman, and C. F. Gmachl, "Mid-infrared quantum cascade lasers," *Nature Photon.* **6**, 432–439 (2012).
13. A. Hasenkampf, N. Kröger, A. Schönhals, W. Petrich, and A. Pucci, "Sensitive trace gas detection with cavity enhanced absorption spectroscopy using a continuous wave external-cavity quantum cascade laser," *Opt. Express* **23**, 5670–5680 (2015).
14. P. Bassan, M. J. Weida, J. Rowlette, and P. Gardner, "Sensitive trace gas detection with cavity enhanced absorption spectroscopy using a continuous wave external-cavity quantum cascade laser," *Appl. Phys. Lett.* **103**, 131114 (2014).
15. S. Mirov, V. Fedorov, I. Moskalev, D. Martyshekin, and C. Kim, "Progress in  $\text{Cr}^{2+}$  and  $\text{Fe}^{2+}$  doped mid-IR laser materials," *Laser & Photon. Rev.* **1**, 21–41 (2010).
16. S. Amarie and F. Keilmann, "Broadband-infrared assessment of phonon resonance in scattering-type near-field microscopy," *Phys. Rev. B* **83**, 045404 (2011).
17. Y. Yu, X. Gai, P. Ma, D.-Y. Choi, Z. Yang, R. Wang, S. Debbarma, S. J. Madden, and B. Luther-Davies, "A broadband, quasi-continuous, mid-infrared supercontinuum generated in a chalcogenide glass waveguide," *Laser Photon. Rev.* **8**, 792–798 (2014).
18. G. Genty, S. Coen, and J. M. Dudley, "Fiber supercontinuum sources," *J. Opt. Soc. Am. B* **24**, 1771–1785 (2007).
19. T. Südmeyer, J. Aus der Au, R. Paschotta, U. Keller, P. G. R. Smith, G. W. Ross, and D. C. Hanna, "Femtosecond fiber-feedback optical parametric oscillator," *Opt. Lett.* **26**, 304–306 (2001).
20. A. Steinmann, B. Metzger, R. Hegenbarth, and H. Giessen, "Compact 7.4 W femtosecond oscillator for white-light generation and nonlinear microscopy," in *Proceedings of CIEO 2011*, (Optical Society of America, 2011), CThAA5.
21. R. Hegenbarth, A. Steinmann, Sergey Sarkisov, and H. Giessen, "Milliwatt-level mid-infrared difference frequency generation with a femtosecond dual-signal-wavelength optical parametric oscillator," *Opt. Lett.* **37**, 3513–3515 (2012).
22. C. Huck, F. Neubrech, J. Vogt, A. Toma, D. Gerbert, J. Katzmann, T. Härtling, and A. Pucci, "Surface-enhanced infrared spectroscopy using nanometer-sized gaps," *ACS Nano* **8**, 4908–4914 (2014).
23. F. Schreiber, "Structure and growth of self-assembling monolayers," *Prog. Surf. Sci.* **65**, 151–257 (2000).
24. D. Lin-Vien, N. W. Colthup, W. G. Fateley, and J. G. Grasselli, *The Handbook of Infrared and Raman Frequencies of Organic Molecules* (John Wiley & Sons, 1991).
25. C. D'Andrea, J. Bochterle, A. Toma, C. Huck, F. Neubrech, E. Messina, B. Fazio, O. M. Marag, E. Di Fabrizio, M. Lamy de La Chapelle, P. G. Gucciardi, and A. Pucci, "Optical nanoantennas for multiband surface-enhanced infrared and raman spectroscopy," *ACS Nano* **7**, 3522–3531 (2013).
26. R. Hegenbarth, A. Steinmann, S. Mastel, S. Amarie, A. Huber, R. Hillenbrand, S. Sarkisov, and H. Giessen, "High-power femtosecond mid-IR sources for s-SNOM applications," *J. Opt.* **16**, 094003 (2014).
27. S. Benschmann, F. Gaussmann, M. Lewin, J. Wuppen, S. Nyga, C. Janzen, B. Jungbluth, and T. Taubner, "Near-field imaging and spectroscopy of locally strained GaN using an IR broadband laser," *Opt. Express* **22**, 22369–22381 (2014).
28. X. G. Xu, M. Rang, I. M. Craig, and M. B. Raschke, "Pushing the sample-size limit of infrared vibrational nanospectroscopy: from monolayer toward single molecule sensitivity," *J. Phys. Chem. Lett.* **3**, 1836–1841 (2012).
29. S. Bagheri, H. Giessen, and F. Neubrech, "Large-area antenna-assisted SEIRA substrates by laser interference lithography," *Adv. Opt. Mater.* **11**, 1050–1056 (2014).

## 1. Introduction

Infrared (IR) spectroscopy allows for unambiguous identification and chemical characterization of molecular species based on their infrared vibrational bands. Unfortunately, such material-specific absorption signals are relatively small, which hampers the spectroscopic detection of minute amounts of substances, e.g., in sensing applications. Also infrared hyperspectral chemical imaging of unstained biological tissue sections [1] with micrometer resolution as it is used in medicine to discriminate between healthy tissue and tumors [2], suffers from small absorption signals and small signal-to-noise ratio (SNR) of conventional IR light sources. This is only possible on reasonable time scales with immense technical effort, e.g. at synchrotron light sources providing 2-3 orders of magnitude brighter IR radiation than thermal light sources [3,4].

One way to overcome these limitations is the use of specially designed metal nanoparticles known as resonant plasmonic nanoantennas [5]. Resonantly excited in the infrared, such nanoantennas confine infrared radiation on the nanometer scale and therefore provide locally high electromagnetic field intensities. Following this approach of surface-enhanced infrared absorption (SEIRA), vibrational signals of molecules located in the plasmonic hotspots can be enhanced up to five orders of magnitude in comparison to conventional infrared spectroscopy [6–8].

Another approach to achieve high intensities and thus enable broadband Fourier-transform infrared (FTIR) spectroscopy of minute sample volumes in reasonable accumulation times is the use of advanced light sources of excellent brilliance [9], defined as the number of photons per second, per unit source area, per unit solid angle and per 0.1% of the central frequency:

$$\text{brilliance} = \frac{\text{photons}}{(\text{s})(\text{mm}^2)(\text{sr})(0.1\% \text{BW})}.$$

Thermal standard sources in FTIR spectroscopy such as globars reach a brilliance of  $\approx 10^{15}$  ph/s/mm<sup>2</sup>/sr/0.1%BW, while high brilliance light sources, for example synchrotrons, achieve  $\approx 10^{18}$  ph/s/mm<sup>2</sup>/sr/0.1%BW in the mid-infrared spectral region [3, 10]. However, synchrotron light sources are extremely cost-intensive due to the high consumption of energy and deliver only a few mW of radiation power in the IR [10]. Additionally, beam-time is rarely available. Besides these incoherent broadband sources, IR laser sources with narrow bandwidth such as CO<sub>2</sub> lasers and quantum cascade lasers (QCLs) [11, 12] are available. Combined with SEIRA such QCLs provide an increased sensitivity in comparison to conventional infrared spectroscopy as recently shown in [13]. Due to their limited bandwidth, sweeping techniques or even several lasers emitting at different wavelengths have to be applied to cover the infrared spectral range of interest, which enable sensitive diffraction-limited IR spectroscopy [14]. However, also the generation of intrinsically broadband and tunable femtosecond radiation with mode-locked laser systems has been shown to be difficult due to the lack of suitable gain media and significant atmospheric absorption in the mid-infrared spectral region [15]. Furthermore, difference frequency generation (DFG) has been employed to generate very broadband infrared supercontinua [16]. Another approach involves supercontinuum generation in nonlinear fibers or waveguides, where recently a brilliance of  $8 \times 10^{20}$  ph/s/mm<sup>2</sup>/sr/0.1%BW has been reached, beating synchrotron sources by 2-3 orders of magnitude [17]. The drawback of such supercontinua, however, is their sensitivity to quantum noise in the process of spectral broadening, which significantly reduces the temporal coherence and leads to excess noise in spectroscopic precision measurements [18].

Optical parametric light sources, such as optical parametric oscillators (OPO) or amplifiers (OPA), provide coherent and easily tunable, extremely brilliant infrared radiation. In these devices, near-infrared femtosecond radiation is converted in nonlinear crystals to the mid-infrared spectral range. With bandwidths of several tens of nanometers in the mid-infrared, individual molecular vibrations can be easily measured, while the continuous tunability ensures the versatility to access other spectral regions.

An important difference between incoherent and coherent sources is the fundamentally different nature of the noise characteristics. Incoherent sources are almost free from intensity noise, while coherent sources exhibit significant intensity noise on different time scales. In particular the sub-millisecond time scale as well as the long term drift properties are relevant for FTIR spectroscopy. Drifts in the intensity or wavelength will directly distort the baseline making it impossible to normalize spectra with reference measurements, while sub-millisecond fluctuations will perturb the acquisition of a single spectrum and will transform into random noise in the spectrum. These disadvantages are quite challenging and have so far hampered the use of coherent sources for FTIR spectroscopy, despite their great advantages in terms of

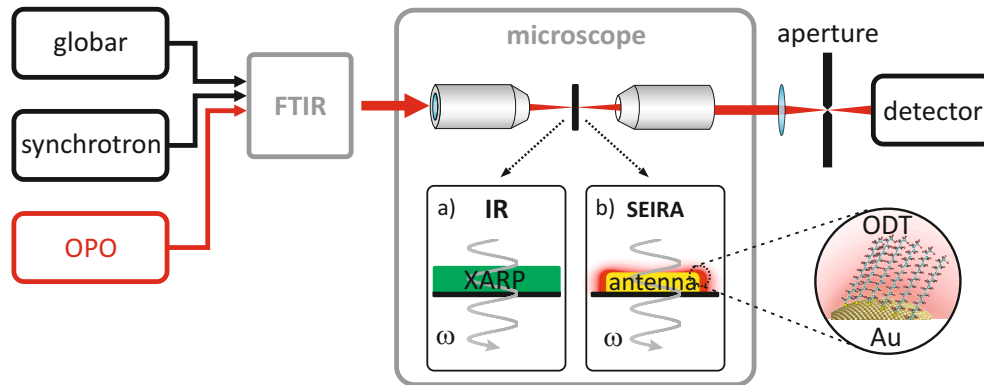


Fig. 1. Schematic illustration of our experiments. Different IR light sources are coupled to a microscope attached to a standard FTIR spectrometer. The performance of our OPO source is demonstrated by (a) conventional IR spectroscopy of a polymer (XARP) with spot sizes down to the diffraction limit and (b) surface-enhanced infrared absorption (SEIRA) of a molecular monolayer (octadecanethiol, ODT) attached to a single plasmonic nanostructure.

brilliance.

In the present work, we overcome these limitations by employing a continuously tunable fiber-feedback OPO emitting highly brilliant and stable IR radiation with bandwidths up to 125 nm in the wavelength range between  $1.4\ \mu\text{m}$  and  $4.2\ \mu\text{m}$ . This radiation is coupled into a conventional FTIR spectrometer and subsequently into an attached microscope, selecting  $\mu\text{m}^2$ -sized areas for infrared spectroscopy [Fig. 1]. To demonstrate highly sensitive and low-noise IR spectroscopy, we investigated micrometer-sized volumes of a polymer [Fig. 1(a)] and employed SEIRA to spectroscopically detect even smaller numbers of molecules [Fig. 1(b)]. The results are compared to FTIR spectroscopy with conventional thermal and synchrotron light sources. We further give a quantitative measure for the fiber-feedback OPO noise performance on different relevant time scales.

## 2. Experimental setup

The high-brilliance infrared source for FTIR spectroscopy is realized by coupling a fiber-feedback OPO [19] into an infrared microscope, which is attached to a conventional FTIR spectrometer [Fig. 2(a)].

The OPO is pumped by an Yb:KGW solid-state oscillator that provides 7 W average power at 1040 nm with a repetition rate of 43 MHz and a pulse duration of 450 fs [20]. The nonlinear frequency conversion takes place in a 10 mm long, temperature controlled, periodically-poled lithium niobate (PPLN) crystal, which is pumped by a 2 – 4 W fraction of the pump laser. The generated signal is collimated with a curved mirror (ROC 150 mm). By employing a half-wave plate and a polarizing beam splitter, a variable share of this signal is fed back into a 4.2 m long SMF-28 fiber that contains most of the intra-cavity optical path length, making the setup extremely compact. Furthermore, the pulses are broadened temporally due to group velocity dispersion in the glass, which leads to a highly stretched feedback pulse. This pulse is delayed in order to be synchronized with the next pump pulse and act as seed for the subsequent parametric amplification step. The high chirp on the feedback pulse ensures both extremely precise wavelength tuning by matching a certain delay as well as excellent wavelength stability, which is further investigated later in this paper. Despite the significant chirp on the feedback, the time-

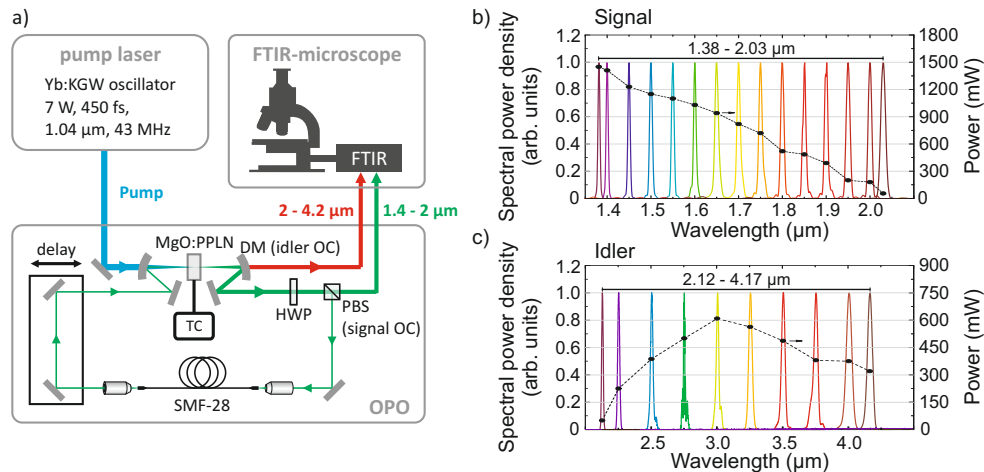


Fig. 2. a) Experimental setup of a fiber-feedback OPO pumped with an Yb:KGW solid-state laser. The generated idler wavelengths, ranging from  $2.12\ \mu\text{m}$  to  $4.17\ \mu\text{m}$ , are coupled into an infrared microscope attached to a standard FTIR spectrometer (TC: temperature control, DM: dichroic mirror, OC: output coupler, HWP: half-wave plate, PBS: polarizing beam splitter). Tuning range and corresponding power level of the OPO signal (b) and idler (c). The spectral range from  $1.38\ \mu\text{m}$  to  $4.17\ \mu\text{m}$  can be completely addressed with typical spectral bandwidths ( $1/e^2$ ) of 20 nm to 125 nm, increasing with center wavelength.

bandwidth product of the emitted signal pulse is on the order of 0.42–0.45 in the whole signal tuning range and can be even lower if low pump power is used. The spectroscopically useful bandwidth ( $1/e^2$ ) is on the order of 20 nm at  $1.4\ \mu\text{m}$  and increases to 125 nm towards  $4\ \mu\text{m}$ . In wavenumbers, this corresponds to approximately  $80\ \text{cm}^{-1}$  over the whole tuning range. Including temperature tuning and changing of the poling period of the multi-channel PPLN crystal from  $27.91\text{--}31.59\ \mu\text{m}$ , a gap free tuning range from  $1.38\text{--}2.03\ \mu\text{m}$  as well as  $2.12\text{--}4.17\ \mu\text{m}$  is achieved [Fig. 2(b) and 2(c)]. Depending on the actual wavelength, the typical power level throughout the tuning range exceeds several hundreds of mW, which is absolutely sufficient for spectroscopic applications, where typically a few mW are required. The system reaches a brilliance of  $3 \times 10^{22}\ \text{ph/s/mm}^2/\text{sr}/0.1\% \text{BW}$  in the idler output, measured at  $3.5\ \mu\text{m}$ , which is about four orders of magnitude greater than that of synchrotron radiation. The tuning range of signal and idler would allow us to extend the spectral range by employing a DFG-scheme [21] into the  $5\text{--}20\ \mu\text{m}$  region with mW power levels.

The high brilliance IR radiation generated with the described fiber-feedback OPO is coupled to a commercially available FTIR spectrometer (Bruker Vertex 80) by means of mirror optics. Subsequently, the IR beam is sent in an infrared microscope (Bruker Hyperion 2000) through a KRS-5 polarizer and focused to the sample by a 36x Cassegrain objective (NA = 0.52). An aperture is inserted after the sample to select  $\mu\text{m}^2$ -sized areas. The transmitted IR radiation is detected with a liquid nitrogen cooled  $250 \times 250\ \mu\text{m}^2$  mercury-cadmium-telluride (MCT) detector. For the synchrotron studies a similar setup is used at the IR2 beamline at the Angström source Karlsruhe (ANKA). Infrared radiation provided by electrons in the storage ring (2.5 GeV and a beam current of 120 mA) is coupled into an infrared microscope (Bruker IRscope II) attached to an FTIR spectrometer (Bruker IFS 66 V/S). A circular aperture in the microscope enables us to select areas down to approximately  $50\ \mu\text{m}^2$  from the natural spot size of the synchrotron beam (diameter of approximately  $20\ \mu\text{m}$ ). All infrared spectra presented in the present study are recorded in transmission geometry with a typical accumulation time of 12

seconds and a resolution of  $2\text{ cm}^{-1}$  with 20 kHz sampling rate unless specified otherwise.

### 3. Vibrational IR spectroscopy

To demonstrate the capability of our fiber-feedback OPO laser source for conventional FTIR spectroscopy, we performed surface-enhanced infrared spectroscopy using resonantly excited gold nanoantennas covered with a molecular monolayer of ODT (thickness 2.8 nm). Employing standard PMMA resist electron beam lithography and lift-off techniques, we fabricated  $100\times 100\text{ }\mu\text{m}^2$ -sized arrays of rectangularly shaped nanostructures (length  $L = 800\text{ nm}$ , height  $h = 50\text{ nm}$ , width  $w = 60\text{ nm}$ ) as well as single nanoantennas ( $L = 900\text{ nm}$ ,  $h = 60\text{ nm}$ ,  $w = 20\text{ nm}$ ). The spacings between the periodically arranged nanoantennas are 40 nm in direction along the long antenna axis and  $1.5\text{ }\mu\text{m}$  perpendicular to it. Details on the selective ODT adsorption on gold surfaces are given in [6, 23]. Excited with light polarized parallel to the long antenna axis ( $E_{\parallel}$ ), the infrared transmittance of such gold nanoantenna arrays (normalized to the bare  $\text{CaF}_2$  substrate) reveals a broadband plasmonic response and enhanced molecular vibrations of ODT ( $3.425$  and  $3.51\text{ }\mu\text{m}$ ) as seen in the global measurements [Fig. 3(a)]. Due to the resonant

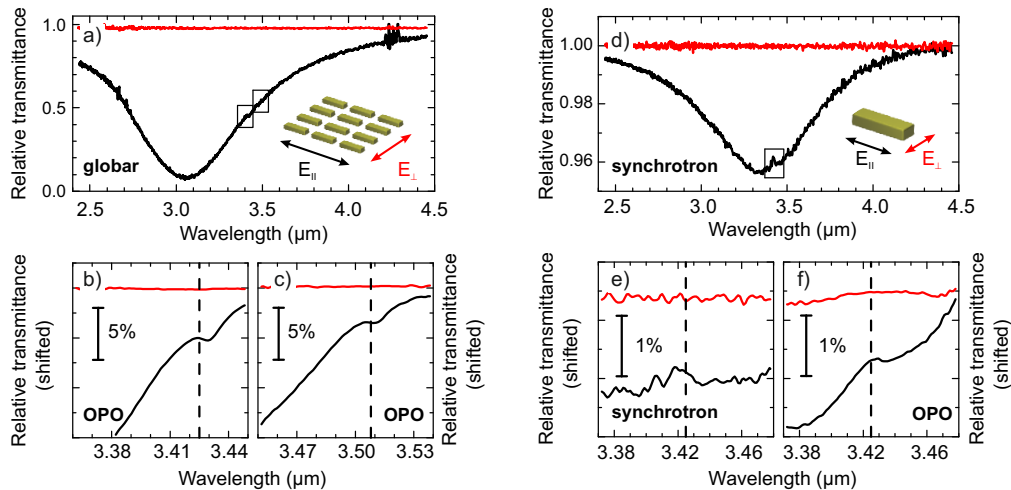


Fig. 3. SEIRA using a nanoantenna array (a-c) and an individual nanoantenna (d-f) covered with a molecular monolayer of ODT. a) Antennas illuminated by a thermal light source (global) feature broadband plasmonic resonances and resonantly enhanced ODT vibrations at  $3.425$  and  $3.51\text{ }\mu\text{m}$  (hardly visible, indicated by boxes) for parallel polarized light ( $E_{\parallel}$ ). IR spectroscopy with the OPO source provides a significantly improved SNR in a 50 times shorter acquisition time  $t$  as seen for the symmetric (b) and asymmetric (c) ODT stretching vibrations (dashed lines). d) Polarization dependent SEIRA with a single ODT-covered nanoantenna illuminated by IR synchrotron radiation. The spectra close to the symmetric ODT vibration ( $3.425\text{ }\mu\text{m}$ , dashed line) acquired with the OPO (f,  $t = 17\text{ min}$ ) provide a significantly improved SNR compared to synchrotron studies (e,  $t = 170\text{ min}$ ).

nature of the plasmonic enhancement, SEIRA signals with Fano-type line-shapes only occur for a good spectral match of the plasmonic and molecular excitations, which is not given for perpendicular polarization ( $E_{\perp}$ ).

However, even for parallel polarization the enhanced molecular vibrations are hardly visible due to the low brilliance of the global source, even for long accumulation times ( $t = 20\text{ min}$ ) and relatively large apertures ( $20\times 20\text{ }\mu\text{m}^2$ ). In contrast to that, the relative transmittance recorded with the fiber-feedback OPO provides a significantly improved SNR in a 50 times reduced

acquisition time as seen for the asymmetric [Fig. 3(b)] and symmetric [Fig. 3(c)] CH<sub>2</sub> stretching vibrations of the ODT molecules [24]. Due to the limited spectral bandwidth of the OPO radiation, which is however sufficient to investigate individual IR vibrational bands, the laser emission wavelength has to be tuned to the respective CH<sub>2</sub> vibration. This reliable tuning is achieved by temperature adjustment of the PPLN crystal and/or cavity tuning of the OPO feedback in less than 2 min and can be easily automatized.

The brilliance of the respective light source becomes even more crucial for infrared spectroscopy with aperture sizes close to the diffraction limit, e.g., SEIRA using single nanoantennas. Such measurements of single nanostructures with thermal light sources are challenging and synchrotrons with 2-3 orders of magnitude brighter IR radiation have to be used [6, 22]. As with our OPO setup, the synchrotron light is coupled to an infrared microscope, which allows the selection of  $\mu\text{m}^2$ -sized areas for relative transmittance spectroscopy of an ODT-covered single gold nanoantenna [Fig. 3(d)]. In agreement with SEIRA using nanostructure arrays, the asymmetric ODT vibration is enhanced by the plasmonic near-field of the resonantly excited antenna and shows the expected polarization dependence. For synchrotron radiation [Fig. 3(e)], the enhanced vibrational signal is slightly larger than the noise, while in the OPO experiments the vibration is clearly visible [Fig. 3(f)]. Spectral differences in the background of the OPO and synchrotron measurements arise from a nonlinear response of the MCT detector, which becomes more pronounced for intensities close to the saturation level as present in the OPO measurements. Both measurements are performed on the very same nanoantenna with similar spot sizes ( $\approx 50 \mu\text{m}^2$ ), but a ten times longer acquisition time for the synchrotron measurements, thus demonstrating the impact of excellent brilliance and stability of the laser beam.

This high quality beam in combination with SEIRA enables low-noise detection of about 10,000 ODT molecules located in the hotspots of a single nanoantenna. We estimated this number assuming an homogeneous ODT adsorption on gold surfaces with an area of  $21.6 \text{ \AA}^2$  per molecule [23] and a SEIRA active area of two times the end faces (20 nm x 60 nm) of the gold antenna according to [25]. To enable spectroscopy below the diffraction limit, our approach could be combined with a scanning near-field optical microscope [26–28].

#### 4. Performance

In microscopic IR spectroscopy typical aperture sizes range from  $100 \times 100 \mu\text{m}^2$  down to the diffraction limit, enabling chemical imaging with micrometer-scale resolution, e.g., of biological tissue sections [1]. However, particularly at small aperture sizes this method suffers from the low brilliance of conventional thermal light sources. As a consequence, the intensity acquired with a standard MCT detector decreases rapidly with shrinking aperture size (see Fig. 4(b), black curves). In contrast, the decrease of the OPO intensity is much less pronounced due to the excellent beam profile. Moreover, the nitrogen cooled MCT detector can always be used at the optimum power level close to saturation by exploiting the  $10^7$  times higher brilliance of the OPO compared to the global. As a further consequence of the high brilliance and excellent stability, especially on the sub-millisecond time scale, the OPO RMS noise level remains almost constant with varying aperture size, whereas the noise level of the global increases by orders of magnitude. This effect is illustrated in Fig. 4(c), where spectrally resolved stability measurements in air are shown. The presented relative transmittance spectra are calculated from two subsequent measurements with typical acquisition times of 12 s each. For larger apertures, both global and fiber-feedback OPO feature a similar RMS noise level whereas for smaller apertures the relative transmission remains smooth for the OPO. However, the RMS noise level of the OPO changes slightly over time, which arises from spectral and intensity drifts on the time scale of seconds and thereby influences successive measurements. The underlying mechanisms are discussed in the introduction. The same behavior is observed in a representative infrared

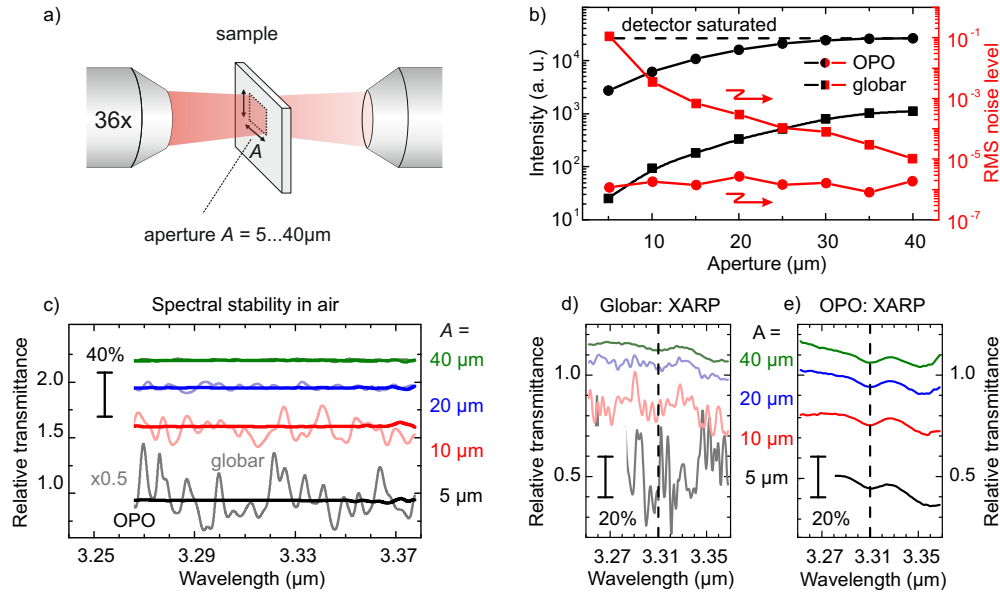


Fig. 4. b) Spectral power density and RMS noise level of a thermal light source (globar) compared to the OPO source in dependence of square aperture (edge length  $A$  given, see a)) demonstrating the excellent focusability of the laser radiation. If the OPO power is maximized at the MCT detector, the spectral power density is only limited by the saturation of the detector (dashed line). For the OPO, the RMS noise level remains almost constant, regardless of the aperture size. c) Relative transmittance (shifted) of air taken with the globar (light colors) and the OPO (intense colors and thick lines) for different square apertures. Relative IR transmittance (shifted) of a  $5\ \mu\text{m}$  thick polymer layer (XARP) measured with the globar (d) and the OPO (e).

absorption measurement of a  $5\ \mu\text{m}$  thick photoresist layer (XARP 3100/10, purchased from *Allresist*) spincoated on a  $\text{CaF}_2$  substrate [29]. As depicted in Fig. 4(d) and 4(e), the relative transmittance of a  $40 \times 40\ \mu\text{m}^2$  area reveals a clearly visible vibrational feature at  $3.31\ \mu\text{m}$  for both sources. For decreasing apertures, however, the vibrational signal is below the noise level in the globar experiments, but remains unchanged in the OPO studies. This confirms the ability of our fiber-feedback OPO to acquire high quality and low noise spectra at the diffraction limit, thus enabling rapid spectroscopic imaging applications with resolution only limited by the diffraction of light. Furthermore, the high power in principle allows the use of low-cost deuterated triglycine sulfate (DTGS) detectors operating at room temperature. In contrast to nitrogen-cooled MCT detectors, DTGS detectors feature a lower sensitivity, but do not suffer from undesired nonlinearities. Such nonlinearities lead to slightly different absolute absorption values in our spectra in comparison to the globar measurements if the detector is exposed to high intensities close to the saturation level.

In more detail, the long term performance of the OPO is evaluated by a series of measurements over 15 min in air, where we investigate the spectroscopically relevant properties of the mid-IR beam [Fig. 5]. We constantly monitor the OPO spectrum with the FTIR detector at one frame every 12 s in order to detect long term drifts that would detrimentally impact spectroscopic measurements by changing the baseline. The analysis is performed by fitting the measured spectrum with a Gaussian peak and extracting the peak intensity, center wavelength and spectral full width at half maximum (FWHM) bandwidth. Fluctuations in peak intensity as low

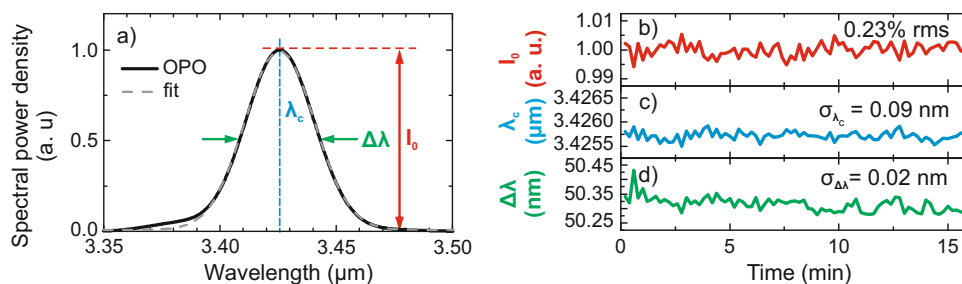


Fig. 5. Spectral power density of the OPO idler (black) and Gaussian fit (grey, dashed) showing the peak intensity  $I_0$ , the center wavelength  $\lambda_c$ , and the spectral bandwidth  $\Delta\lambda$  (a). As a measure of stability, these quantities are monitored with the FTIR spectrometer over 15 min with one frame every 12 s, using the DTGS detector. The peak intensity shows RMS noise of 0.23% RMS (b), while the variances of center wavelength (c) and spectral bandwidth (d) are 0.09 nm and 0.02 nm, respectively. No active stabilization of the OPO is employed.

as 0.23% RMS are achieved. Excellent spectral stability with a variance of less than 0.09 nm in center wavelength and about 0.02 nm in spectral bandwidth is observed. There are almost no drift features visible. These values are on the level of the near-infrared solid-state pump laser, and, with our tunable OPO, available over a broad spectral range.

## 5. Conclusion and outlook

We demonstrate ultra-sensitive infrared spectroscopy near the diffraction limit by coupling a high-brilliance fiber-feedback OPO light source to a conventional FTIR spectrometer. Combining the setup with surface-enhanced infrared spectroscopy, we detect approximately 10,000 ODT molecules attached to a resonantly excited *single* gold nanoantenna in a ten times faster acquisition time compared to synchrotron light sources. This excellent performance is enabled by the four orders of magnitude higher brilliance as well as the low-noise nature of the tabletop OPO with respect to both the sub-millisecond time scale as well as the long term drift.

In order to access the molecule-specific fingerprint region, which is relevant in almost all spectroscopic applications, we plan to extend the accessible spectral range to 5–12  $\mu\text{m}$ . This will enable high speed infrared spectroscopy in chemistry, biology, medicine and pharmaceutical science even in standard laboratories and will allow for broadband spectroscopic scanning near-field optical microscopy.

## Acknowledgments

The authors gratefully acknowledge financial support by ERC Advanced Grant COMPLEX-PLAS as well as DFG, BMBF, GIF, Carl Zeiss foundation, and MWK Baden-Württemberg and the Baden-Württemberg Stiftung (PROTEINSENS, Spitzenforschung II). This work was supported by the German Research Foundation (DFG) within the funding program Open Access Publishing. We thank D. Floess for nanofabrication and J. Weis for cleanroom access. We acknowledge the Synchrotron Light Source ANKA for provision of instruments at the IR2 beamline and we would like to thank D. Moss, Y-L. Mathis and M. Süpfle for their assistance. We further thank Mr. G. Zachmann (Bruker Optik GmbH) for fruitful discussions.